ADVANCED MATERIALS INTERFACES
www.advmatinterfaces.de

Check for updates

Interplay between Charge Injection, Electron Transport, and Quantum Efficiency in Ambipolar Trilayer Organic Light-Emitting Transistors

Salvatore Moschetto, Emilia Benvenuti, Hakan Usta, Resul Ozdemir, Antonio Facchetti, Michele Muccini, Mario Prosa, and Stefano Toffanin**

The fascinating characteristic of organic light-emitting transistors (OLETs) of being electrical switches with an intrinsic light-emitting capability makes them attractive candidates for a wide variety of applications, ranging from sensors to displays. To date, the OLET ambipolar trilayer heterostructure is the most developed architecture for maximizing device performance. However, a major challenge of trilayer OLETs remains the inverse correlation between external quantum efficiency and brightness under ambipolar conditions. The complex interconnection between electroluminescent and ambipolar charge transport properties, in conjunction with the limited availability of electron transport semiconducting materials, has indeed hampered the disruptive evolution of the OLET technology. Here, an in-depth study of the interplay of the key fundamental features that determine the device performance is reported by exploring electron transport semiconductors with different properties in ambipolar trilayer OLETs. Through the selection of compounds with tailored chemical structures, the relation between intrinsic optoelectronic characteristics of the electron transport semiconductor, energy level alignment within the structure, and morphological features is unraveled. Furthermore, the introduction of a suitable electron injector at the emissive/semiconducting layers interface sheds light into the bidimensional nature of OLETs that is a distinguishing factor of this class of devices with respect to prototypical organic light-emitting diodes.

1. Introduction

Organic semiconductors (OSCs) have attracted considerable interest for several advantages such as tuning material properties via chemical synthesis, mechanical flexibility, and thin films processing by cost-effective techniques.[1–4] The penetration of OSCs into everyday life has emerged in the past decade by the widespread usage of organic light-emitting diode (OLED)-based displays.[5] The use of OLEDs as an alternative to conventional liquid crystal displays is promoted by a series of technological benefits such as low power consumption, lightweight, high brightness, high luminous efficiency, and fast response time.[6] An OLED is a nanometer-thick semiconductor device that is capable of generating photons when a suitable electrical bias is applied. However, the vertical architecture of OLEDs, which dictates that photons pass through at least one electrode, poses a significant limitation to the device characteristics as a result of optical cavity effects and limited electrode transparency.[7,8] In this context, organic light-emitting transistors (OLETs) have gained attention in the past decade thanks to their ability to integrate logical switching functionality of transistors with light emission through a simple planar architecture.[6,9,10] Most importantly, light emission could be tuned to occur far from metal electrodes.[11] With respect to OLEDs, a potential increase of the optical efficiency is therefore predicted since undesired quenching and optical effects could be avoided. In addition, the planar OLET structure offers a key feature for the realization of integrated systems with complex functions.[12,13] In OLETs,

S. Moschetto, E. Benvenuti, M. Muccini, M. Prosa, S. Toffanin
Institute of Nanostructured Materials (ISMN)
National Research Council (CNR)
Via P. Gobetti 101, Bologna 40129, Italy
E-mail: mario.prosa@cnr.it; stefano.toffanin@cnr.it

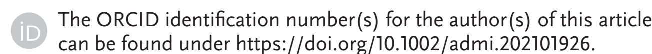
The ORCID identification number(s) for the author(s) of this article can be found under https://doi.org/10.1002/admi.202101926.

© 2022 The Authors. Advanced Materials Interfaces published by Wiley-VCH GmbH. This is an open access article under the terms of the Creative Commons Attribution License, which permits use, distribution and reproduction in any medium, provided the original work is properly cited.

DOI: 10.1002/admi.202101926

H. Usta, R. Ozdemir
Department of Nanotechnology Engineering
Abdullah Gül University
Kayseri 38080, Turkey

A. Facchetti
Department of Chemistry and the Materials Research Center
Northwestern University
2145 Sheridan Road, Evanston, IL 60208-3113, USA

A. Facchetti
Flexterra Inc.
8025 Lamon Avenue, Skokie, IL 60077, USA

A. Facchetti
Laboratory of Organic Electronics
Department of Science and Technology
Linköping University
Norrköping, SE-60174, Sweden

© 2022 The Authors. Advanced Materials Interfaces published by Wiley-VCH GmbH

21967350, 2022, 5, Downloaded from https://onlinelibrary.wiley.com/doi/10.1002/admi.202101926 by CNR Bologna, Wiley Online Library on [19/12/2024]. See the Terms and Conditions (https://onlinelibrary.wiley.com/terms-and-conditions) on Wiley Online Library for rules of use; OA articles are governed by the applicable Creative Commons License

the double function of electrical amplification and optical emission not only simplifies the driving circuitry, but it also enables a cost-effective manufacturing process. The majority of recently reported OLETs comprise a single ambipolar semiconducting layer endowed with electroluminescent characteristics.[14–17] Under ambipolar conditions, the recombination of opposite charges occurs within the transistor channel and, given the in-plane charge diffusion, the emission region is as large as a few tens of micrometers, thus making OLETs intrinsically micrometer emitters.[9,18] Furthermore, the use of three electrical terminals to balance ambipolarity allows for tuning the location of the emission zone across the transistor channel.[11] Despite these outstanding properties, OLET development has suffered from the low intensity of light emission under ambipolar operation due to the challenge of obtaining OSCs with both efficient ambipolar charge conduction and electroluminescent emission in the solid state. In this context, a breakthrough was achieved by introducing the trilayer OLET architecture,[10] in which the required optical and electrical characteristics are provided by three different layers. This device structure, where the emissive layer (EML) is sandwiched between an n-type and a p-type semiconducting layers, has exhibited high external quantum efficiency (EQE) values that outperformed those of the corresponding OLEDs. However, the weak brightness of these devices remains to be addressed. To this end, advanced strategies have been proposed such as the use of a conjugated polyelectrolyte as an electron-injection layer (EIL) at the OSC/electrode interface to improve brightness by impeding non radiative recombinations.[19] Alternatively, Ullah et al. have developed asymmetric trilayer structures in which top electrodes are non-planar.[20] While both approaches have drastically improved the OLET trilayer performance, the devices have lost their key characteristic of being able to move the emission stripe within the OLET channel via tuning electrical bias, which is a distinguishing feature of the OLET technology. Compared to the vertical operation of OLEDs, trilayer OLETs are indeed bidimensional devices. Under ambipolar regime, opposite charges flow horizontally across the parallel semiconducting layers to be injected vertically into the EML, which is sandwiched between them. The correlation between optoelectronic characteristics of each layer and the energy level alignments within the device structure must be optimal to ensure a good ambipolar field-effect behavior and an efficient light emission process. The relatively small library of OSCs in the literature with high n-type mobility and suitable energy levels, especially when compared with p-type OSCs,[21–28] is one of the main reasons why most studies focus on a limited number of OLET devices with similar components.[3] A balance between n-type and p-type charge transports in OLETs is still a significant limitation to efficient devices. Charge transport of OSCs used in OLETs has been mostly investigated in structures where the semiconducting layer is deposited onto a flat surface, as is typical for single layer OFETs. However, when an OSC is deposited on top of an EML in a multilayered architecture, the interface between the EML and the top-lying semiconducting layer could have a serious impact on both energy levels and electrical characteristics of the semiconducting layer.[10] Energy level alignments, morphological properties, and intrinsic optoelectronic properties of each layer of the multi-layered stack all contribute to the operation of trilayer OLETs. As a result, the complex mechanisms and their interplay under ambipolar regime are not fully mastered. Although theoretical simulations have provided mechanistic insights into OLET operation,[11,29] their full potential, especially with regards to brightness, is yet to be studied. In this regard, a comparative study that analyzes in-depth the optoelectronic characteristics of ambipolar trilayer OLETs as a function of the properties of the EML/n-type semiconductor (n-OSC) interface has never been carried out. An optimal design of the device structure would only be possible with a thorough knowledge of these parameters that govern the OLET operation.

Herein, we fabricated, analyzed, and compared ambipolar trilayer OLETs based on three different n-OSCs, ditridecylperylene-3,4,9,10- tetracarboxylic diimide (P13), (2,5-bis(4-(perfluorooctyl)phenyl)thieno-[3,2-b]thiophene (N-F2-6), and α,ω-diperfluorohexyl-quaterthiophene (DFH-4T), which serve as the top-lying semiconductor layer with varied structures, electron mobilities, and energy levels. The use of these n-OSCs is expected to induce crucial changes in both the electrical and optical characteristics of the corresponding OLETs, as well as in the electron injection process into the EML. To further identify the contribution of the EML/n-type semiconducting interface to the overall device characteristics, an interlayer was also implemented.[30] Specifically, an EIL based on a thin film of bathophenanthroline (bphen) was deposited between the EML and the n-OSC, and its effects on the morphological characteristics of the n-OSC and the optoelectronic characteristics of the device were investigated. The EIL is proved to play a critical role to i) favor vertical injection of electrons, flowing horizontally across the n-OSC, into the EML to meet the vertical flux of holes and ii) block the extraction of holes from the EML to the n-OSC to increase the electroluminescence efficiency. This study helps in understanding the basic mechanisms of trilayer OLETs in terms of charge transport and light generation processes, as they are strongly dependent on the interplay of energy levels alignment, intrinsic molecular properties, and morphological packings. In addition, the implementation of a vertical charge injection interlayer in a bidimensional device clearly highlights the similarities and differences between the OLED and the OLET technology.

2. Results and Discussion

2.1. Design and Material Selection of Trilayer OLETs

Three different trilayer OLETs are investigated by implementing P13, N-F2-6, or DFH-4T n-OSCs on top of a bilayer OLET structure (**Figure 1**a) comprising 2,7-dioctyl[1]benzothieno[3,2-b][1]benzothiophene (C8-BTBT) as the p-type charge transport material and tris(8-hydroxyquinoline)aluminum(III) (Alq_3) doped with a near infrared (NIR) emitter Pt(II)–tetraphenyltetrabenzoporphyrin (Pt(tpbp)) as the host-guest EML.[31] In the selection of EML, the use of Pt(tpbp) as a dopant attracted particular interest on the basis of its NIR electrophosphorescence, making the corresponding device suitable for sensing and night-vision applications.[4] This host-guest EML has been used in OLEDs for reaching EQE values as high as 6%.[31] All OLETs were fabricated on a transparent glass/indium tin oxide (ITO)/poly(methyl methacrylate) (PMMA) substrate promoting the photon emission toward top and bottom directions. All layers were deposited by thermal evaporation in order to minimize

 © 2022 The Authors. Advanced Materials Interfaces published by Wiley-VCH GmbH

21967350, 2022, 5, Downloaded from https://onlinelibrary.wiley.com/doi/10.1002/admi.202101926 by CNR Bologna, Wiley Online Library on [19/12/2024]. See the Terms and Conditions (https://onlinelibrary.wiley.com/terms-and-conditions) on Wiley Online Library for rules of use; OA articles are governed by the applicable Creative Commons License

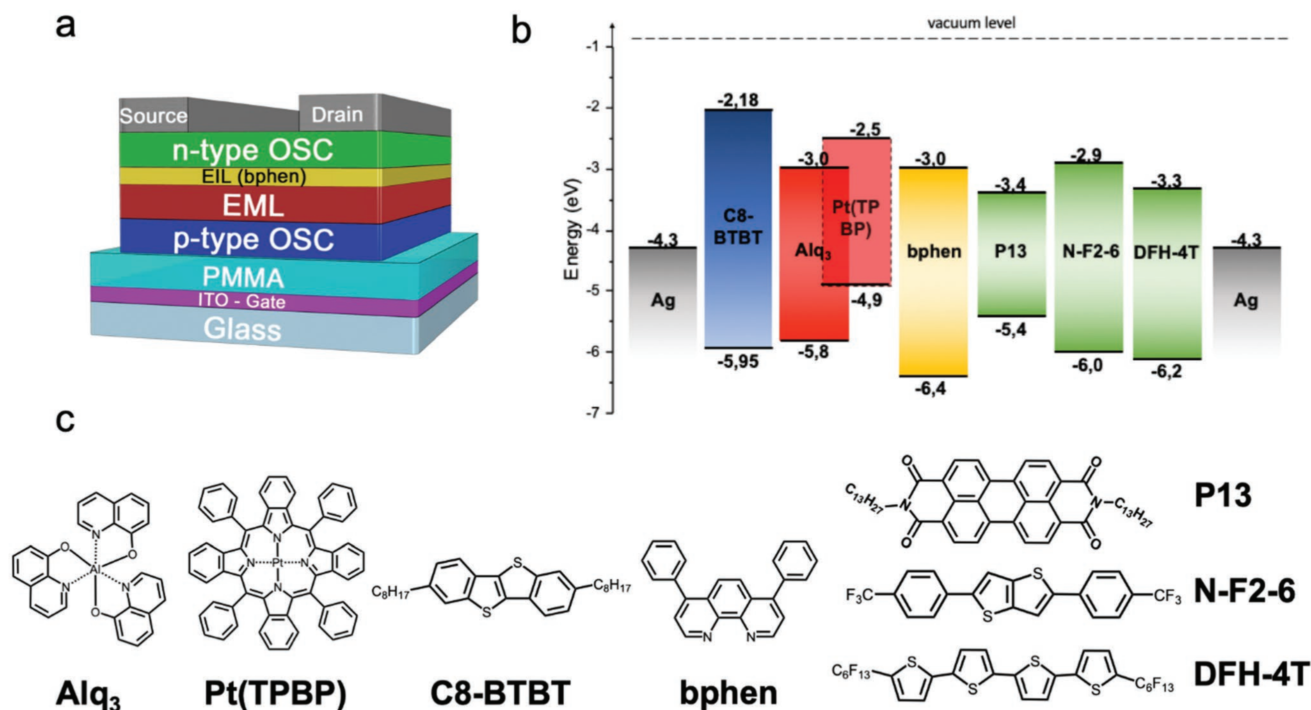

Figure 1. a) Device structure of trilayer OLETs comprising P13, N-F2-6, and DFH-4T as n-OSC. Reference trilayer OLETs do not include any bphen interlayers. b) Energy level diagram of all employed materials in the trilayer OLET structures. c) Chemical structures of the molecular compounds used in this work.

the presence of non-rated factors in the comparative analysis. Energy levels of the trilayer devices are shown in Figure 1b.

In the proposed device structure, efficient p-type operation is guaranteed by the excellent energy alignment of the highest occupied molecular orbital (HOMO) of C8-BTBT with respect to that of Alq_3, which ensures a barrier-less hole injection from C8-BTBT to the host-guest EML. In the selection of the n-OSC, one of the key factors is to guarantee a good energy level alignment within the OLET structure. A high n-type mobility is also recommended in order to guarantee good ambipolar behavior of the trilayer heterostructure. Intrinsic materials properties or data from literature are typically considered in the evaluation of the n-OSC properties. Nevertheless, morphological modifications of the n-OSC in the multilayered stack of materials could greatly affect the semiconductor properties of the compound.

Among state-of-the-art n-OSCs, P13 attracts particular attention for its good electron mobility of 0.1 $cm^2\ V^{-1}\ s^{-1}$,[32] which has led to high performing OFETs with unipolar and ambipolar characteristics.[33,34] In addition, thin films of P13 have shown a well ordered morphology as a result of strong intermolecular interactions in the solid phase.[32] This is particularly important to guarantee an efficient charge transport when they are deposited on a multi-stack architecture. Nevertheless, P13 has a suboptimal energy level alignment within the trilayer OLET structure, as shown in Figure 1b. A non-negligible energy offset between the lowest unoccupied molecular orbitals (LUMOs) of Alq_3 and P13 suggests a poor electron injection efficiency into the EML. Furthermore, relatively high HOMO energy level of P13 with respect to that of Alq_3 favors undesirable hole extraction from the EML. The optimal charge transport behavior of P13, in combination with a suboptimal energy level alignment, allows for studying the role of injection barriers in OLETs.

In order to fulfill the requirements on the energy level alignment of the trilayer OLET structure, an n-OSC characterized by a high LUMO level, preferably greater than that of Alq_3, is desired to guarantee an efficient electron injection into the EML. Therefore, we selected the wide band gap n-OSC N-F2-6, which has HOMO and LUMO levels of –6.0 and –2.9 eV, respectively (Figure 1b). The drawback of using N-F2-6 arises from its relatively poor electron mobility (μ_e) of about 8×10^{-3} $cm^2\ V^{-1}\ s^{-1}$,[35] that should negatively impact ambipolar characteristics of the device. A comparative analysis between N-F2-6- and P13-based trilayer OLETs therefore allows for understanding the role of energy level alignments in OLET structures with respect to ambipolarity. It is clear that the presence of multiple constraints in the design of ambipolar trilayer OLETs requires a balance between morphological, electrical, and energy characteristics of the n-OSC. In this regard, DFH-4T has exhibited μ_e as high as 0.5 $cm^2\ V^{-1}\ s^{-1}$ in single-layer OFETs[10] and, when compared with P13, it is characterized by a lower HOMO level that ensures an effective hole blocking effect at the interface with the EML (Figure 1b). Despite the presence of LUMO energy offset at the interface with the EML, DFH-4T has the highest electron mobility among the selected n-OSCs herein, which is very similar to the hole mobility of C8-BTBT, thus facilitating ambipolarity in the trilayer OLET. Moreover, large 2D island-based morphology of DFH-4T films,[36] arising from strong long-range molecular interactions, should enable the fabrication of efficient multilayered devices.

Mechanisms occurring at the EML/n-OSC interface are crucial to guarantee an optimal device operation under ambipolar

 © 2022 The Authors. Advanced Materials Interfaces published by Wiley-VCH GmbH

21967350, 2022, 5, Downloaded from https://onlinelibrary.wiley.com/doi/10.1002/admi.202101926 by CNR Bologna, Wiley Online Library on [19/12/2024]. See the Terms and Conditions (https://onlinelibrary.wiley.com/terms-and-conditions) on Wiley Online Library for rules of use; OA articles are governed by the applicable Creative Commons License

conditions.[37] The critical role of this interface is to enable the switch from a horizontal flux of electrons, flowing across the n-OSC layer, to the vertical direction to be injected into the EML. In this regard, we introduce an energetically suitable bphen-based EIL (HOMO = −6.4 eV and LUMO = −3.0 eV) that favors electron injection process into the EML while avoiding undesirable hole extraction into the n-OSC layer (Figure 1), which is expected to balance the density of both charge carrier types within the EML.[38] Also, the EIL could act as a physical spacer to avoid undesirable non-radiative charge-exciton recombinations at the EML/n-OSC interface. As a result of complex interplay of factors involved in the operation of trilayer OLETs, a single EIL material is selected for all OLET devices to have a better comparative analysis. Especially, the LUMO of bphen (−3.0 eV) ensures the same energy offset at the EML/n-OSC interface with respect to the reference trilayer device without any EIL.

2.2. EIL in Bilayer OLETs

As a preliminary means of verification, the effectiveness of bphen to vertically inject electrons into the EML is investigated in benchmark bilayer OLETs.

Bilayer OLETs were fabricated in ITO/PMMA/C8-BTBT/Alq_3:Pt(TPBP)/bphen/Ag and ITO/PMMA/C8-BTBT/Alq_3:Pt(TPBP)/Ag (Figure 1a) device structures with and without bphen-based EIL, respectively.

Both devices show a quadratic increase of I_{ds} as a function of V_{gs} (**Figure 2**a), in agreement with the typical transistor characteristics operating in the saturation regime, as it is also highlighted by the p-type output characteristics of both OLETs (Figure S1, Supporting Information). Under that operational regime, the hole-mobility (μ_h) and the threshold voltage ($V_{th(h)}$) are respectively 4×10^{-2} cm^2 V^{-1}s^{-1} and −46 V for the reference bilayer device, and 8×10^{-2} cm^2 V^{-1}s^{-1} and −62 V for the bphen-based bilayer OLET. The slight increase of $V_{th(h)}$ for the device having the EIL is likely because the EIL acts as a hole blocking layer (HBL) from the source electrode to the p-type OSC layer.[39] The hole blocking effect at the drain electrode improves the number of charge recombination events, thus likely reducing the electrical resistance of the device, and doubling the μ_h with respect to the reference device without EIL. As a result, the optical performance is expected to be improved by using a bphen interlayer. The EQE of both devices is calculated as an indicator of the efficiency to convert free charges into photons. Because of the unipolar operation, the vertical flow of holes in proximity of the drain electrode favors charge recombination events to occur in that region of the EML. As shown in Figure 2b, both OLETs show an increase of the EQE as a function of V_{gs}, as it typically occurs in unipolar OLETs. Specifically, the EQE increases from 0.12% for the reference device to 0.50% when the bphen interlayer is included in the device. Possible morphological contributions to the EIL operation could be ignored since the growth of the bphen layer is not affected by the EML layer underneath (Figure S2, Supporting Information). It is clear that the presence of bphen as EIL in a well-designed unipolar bilayer OLET guarantees a more effective electron injection process, from the drain electrode to the EML, with respect to the reference bilayer OLET.

2.3. Trilayer OLETs

N-OSC incorporation into the bilayer OLET is expected to promote ambipolar characteristics that, as a function of the applied bias, should allow moving the light emitting region from the drain electrode toward the transistor channel. To this end, three different n-OSCs (P13, N-F2-6, and DFH-4T) were studied as discussed previously. The main figures of merits for the resulting trilayer OLETs, with and without bphen, are reported in **Table 1**.

First, P13 was deposited onto the bilayer structure, which yields a trilayer OLET structure with good ambipolar behavior (**Figure 3**a). A V-shaped transfer curve is evident during p-channel scan in the saturation regime, which indicates an ambipolar operation.[40] The n-type contribution to the ambipolarity is confirmed by the presence of locus and output characteristics under positive gate polarization (Figure S3a,c, Supporting Information). As evidenced by the presence of a clear pinch-off point, n-type output characteristics at $V_{gs} \geq 80$ V (inset of Figure S3c, Supporting Information) clearly shows n-channel formation. Accordingly, p-type output curves in the saturation regimes at $V_{gs} \leq |-80$ V| (Figure S3b, Supporting Information) exhibit an increase of I_{ds} with increasing V_{ds}, as typically occurs in ambipolar OFETs.[26,41,42] Despite the good n-type characteristics of

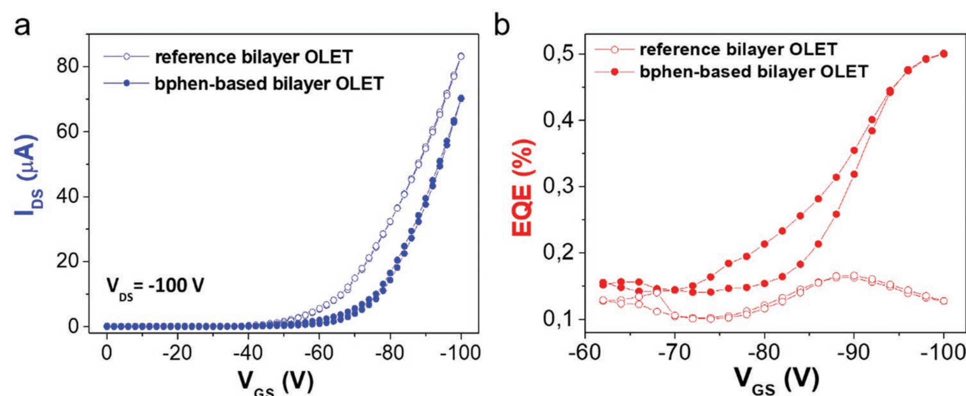

Figure 2. a) P-type transfer curves in saturation regime of bilayer OLETs with (filled blue dots) and without (empty blue dots) any bphen interlayer; b) EQE as a function of V_{gs}, at V_{ds} = −100 V, of bilayer OLETs respectively with (filled red dots) and without (empty red dots) bphen interlayer.

© 2022 The Authors. Advanced Materials Interfaces published by Wiley-VCH GmbH

21967350, 2022, 5, Downloaded from https://onlinelibrary.wiley.com/doi/10.1002/admi.202101926 by CNR Bologna, Wiley Online Library on [19/12/2024]. See the Terms and Conditions (https://onlinelibrary.wiley.com/terms-and-conditions) on Wiley Online Library for rules of use; OA articles are governed by the applicable Creative Commons License

Table 1. Summary of the main figures of merit of trilayer OLETs of this study.

n-OSC in trilayer OLETs	n-mobility [cm^2 V^{-1} s^{-1}]*	$V_{th(e)}$ [V]*	$I_{dsmax(e)}$ [μA]**	p- mobility [cm^2 V^{-1} s^{-1}]*	$V_{th(h)}$ [V]*	$I_{dsmax(h)}$ [μA]**	EL_{max} [nW]**
P13	$1,7 \times 10^{-2}$	32,7	180	$1,1 \times 10^{-1}$	–19,3	427	96
bphen/P13	$1,6 \times 10^{-2}$	48,4	214	$6,3 \times 10^{-3}$	–80,4	125	34
N-F2-6	–	–	11	$1,4 \times 10^{-1}$	–39,3	315	2570
bphen/N-F2-6	–	–	–	$3,2 \times 10^{-1}$	–44,5	640	4000
DFH-4T	–	–	–	$1,3 \times 10^{-1}$	–11,7	600	1250
bphen/DFH-4T	$6,5 \times 10^{-3}$	57,0	8	$2,3 \times 10^{-1}$	–30,0	674	815

*Calculated from saturation transfer curves in the saturation regime; **at $|V_{ds}| = |V_{gs}| = 100$ V.

trilayer OLETs comprising P13 as the n-OSC, the μ_e is one order of magnitude lower than the benchmark P13-based OFETs,[32] which are 0.017 and 0.3 cm^2 V^{-1} s^{-1}, respectively (Table 1). The molecular packing of P13 is slightly influenced by the underlying layers, and it seems to mimic the ring-shaped morphology of the C8-BTBT layer (Figures S2a,S4a, Supporting Information).[35]

The p-type and n-type characteristics of trilayer OLETs are well-balanced when P13 is used as the n-OSC. Nevertheless, the devices have significant limitations in terms of the optical performance, which is maximized only under unipolar operation ($V_{gs} = V_{ds} = -100$ V) at which the EQE is around 0.016% (Figure 3b) and the optical power of emission is as low as 96 nW (Table 1). On the basis of these results, it is evident that non-radiative recombination dominates over radiative events and the excited states of the EML are not populated. From frontier orbital energetics perspective, these poor OLET performance could be explained by the relatively higher HOMO and lower LUMO levels of P13 with respect to those of Alq_3, which hinders the confinement of excitons in the bulk of the EML.

A bphen interlayer is also inserted at the EML/P13 interface serving as the HBL. Holes are expected to be confined in the Alq_3 layer because of the energy offset between the HOMO of bphen (–6.4 eV) and that of P13 (–5.4 eV) (Figure 1b). We first verified that the implementation of the bphen interlayer does not affect the morphological characteristics of the P13 layer (Figure S4, Supporting Information). The insertion of bphen interlayer results in a device that has less pronounced p-type characteristics with respect to the reference trilayer OLET, as evidenced by the V-shaped transfer characteristics under p-type polarization showing a lower I_{ds} at $V_{gs} = -100$ V ($I_{dsmax(h)}$) (Figure 3a). An enhanced n-type behavior is evident in the output characteristics (Figure S3, Supporting Information). In particular, while p-type output curves (Figure S3d, Supporting Information) show the absence of a p-type saturation regime for $V_{gs} < |-80\text{ V}|$, n-type output curves (Figure S3e, Supporting Information) reach the pinch-off point at values of $V_{gs} \geq 20$ V. This is in contrast with what occurs in the reference device, which showed the pinch-off point at $V_{gs} \geq 80$ V (Figure S3c, Supporting Information, inset). The different electrical characteristics between the reference and the bphen-based trilayer OLETs are mainly due to limited hole injection from the source electrode to the C8-BTBT layer due to bphen's deep HOMO level. This process tips the scale of ambipolarity toward the n-type operation in bphen-based OLETs. Accordingly, as shown in Table 1, the presence of bphen drastically reduces the emission intensity with three times lower optical power.

However, the EQE value for bphen-based OLETs remains almost the same as the reference trilayer device (Table 1) accounting 0.012% and 0.014% for the reference and the bphen-based devices, respectively. Here we note that the EQEs for both P13-based OLETs are maximized under unipolar conditions ($V_{gs} = V_{ds} = -100$ V) (Figure 3b), indicating that the light emission is mainly driven by the flux of holes. The presence of bphen has negligible influence on the process of radiative recombination, which is limited by the energy barrier for the injection of electrons into the EML arising from the deep LUMO level of P13. The implementation of P13 in trilayer OLETs highlights the crucial role that the energy level alignment has on the optical characteristics of the devices.

In this regard, the energy level requirement between n-OSC and EML is fulfilled by implementing N-F2-6 in trilayer OLETs.

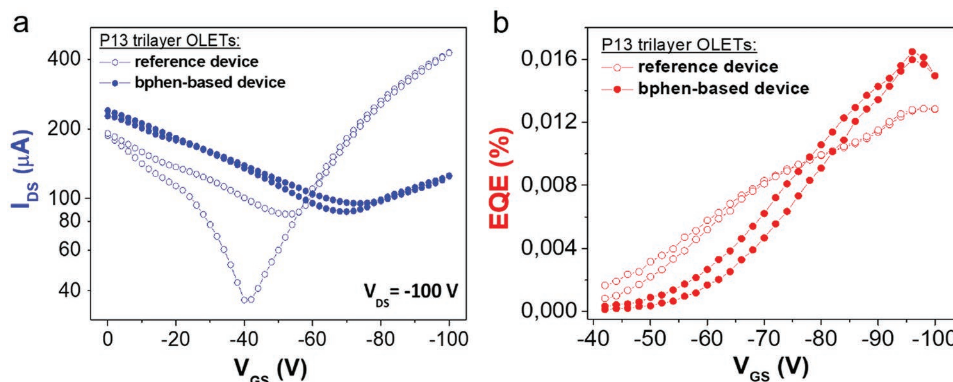

Figure 3. a) P-type transfer curves in saturation regime of P13-based trilayer OLETs with (filled dots) and without (empty dots) bphen interlayer; b) EQE curves of P13-based trilayer OLETs with (filled dots) and without (empty dots) bphen interlayer.

 © 2022 The Authors. Advanced Materials Interfaces published by Wiley-VCH GmbH

21967350, 2022, 5, Downloaded from https://onlinelibrary.wiley.com/doi/10.1002/admi.202101926 by CNR Bologna, Wiley Online Library on [19/12/2024]. See the Terms and Conditions (https://onlinelibrary.wiley.com/terms-and-conditions) on Wiley Online Library for rules of use; OA articles are governed by the applicable Creative Commons License

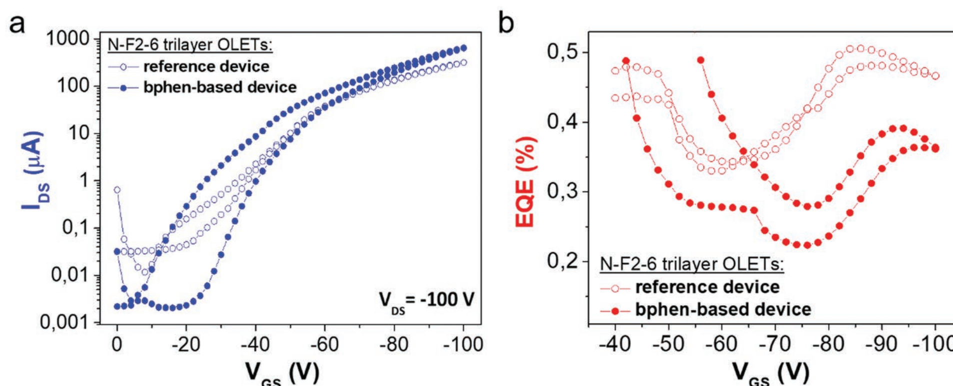

Figure 4. a) P-type transfer curves in saturation regime of N-F2-6-based trilayer OLETs with (filled dots) and without (empty dots) bphen interlayer; b) EQE curves of N-F2-6-based trilayer OLETs with (filled dots) and without (empty dots) bphen interlayer.

The high LUMO level of N-F2-6 (–2.9 eV) indeed greatly matches that of Alq_3 (–3.0 eV) to promote electron injection into the EML. Interestingly, the reference trilayer device employing N-F2-6 shows high optical performance as indicated by the EQE that reaches the maximum value of 0.5% and an emission optical power of 2570 nW under unipolar conditions (V_{gs} = V_{ds} = –100 V) (**Figure** 4b). This EQE is similar to that of bphen-based bilayer OLETs (Figure 2b), which is an indirect confirmation for the optimal energy alignment within the OLET structure.

However, the significant imbalance between electron and hole transport of N-F2-6 and C8-BTBT,[35] respectively, results in unipolar operation of the resulting trilayer OLET, as evidenced by the absence of any V-shape in the transfer characteristics under negative biases (Figure 4a). Indeed, these devices exhibit poor n-type characteristics as highlighted by a low $I_{dsmax(e)}$ (Table 1) that hinders the estimation of $V_{th(e)}$ and μ_e. Locus characteristics can be barely evidenced under positive polarization (Figure S5a, Supporting Information), and output curves show only a p-type behavior for both p- and n-type characterizations (Figure S5, Supporting Information) thus confirming the poor ambipolarity of the device. Specifically, n-type output curves are mostly characterized by residual p-type characteristics (Figure S5c, Supporting Information, inset), and the n-type saturation regime is not reached even at a bias as high as V_{gs} = 100 V.

As a consequence of the poor electron transport properties, reference N-F2-6-based OLETs are mostly dominated by the flux of holes, thus resulting to be unipolar devices. In addition, the similarity of their characteristics to those of bphen-based bilayer OLETs suggests that N-F2-6 functions as an EIL, rather than an n-OSC. A thin film of bphen is implemented at the EML/n-OSC interface to evaluate any possible impacts on the n-type behavior of the n-OSC and the ambipolarity of trilayer OLETs as a result. The insertion of the bphen interlayer in the OLET structure has a great impact on the OLET electrical characteristics. However, the n-type electrical behavior of the device has further deteriorated with respect to the reference trilayer device despite an improved ambipolarity was sought. In particular, no n-type locus characteristics are evidenced (Figure S5a, Supporting Information), and both p- and n-type output characteristics are similar to those of the reference trilayer device (Figure S5, Supporting Information). Moreover, p-type transfer curves (Figure 4a) show a more pronounced hysteresis with respect to the reference trilayer device, thus likely indicating a charge accumulation process at the N-F2-6/bphen or EML/bphen interface due to the presence of the bphen interlayer.

This assumption is confirmed by the EQE of the bphen-based OLETs (Figure 4b), which decreases from 0.50% for the reference device to 0.36% (at V_{gs} = –85 V). To investigate the cause of the relatively poor electron transport characteristics of N-F2-6 in the trilayer structure, morphological analyses are carried out (Figure S6, Supporting Information). However, the underlying multilayered stack is found to have no effects on the solid-state organization of the N-F2-6 layer (Figure S6a, Supporting Information), which shows a needle-like morphology that is i) independent of the presence of a bphen interlayer (Figure S6b, Supporting Information), and ii) similar to the molecular organization occurring on flat surfaces.[35] Therefore, the cause of the deterioration in the device performance when using a bphen interlayer is probably due to the formation of a new interface (i.e., N-F2-6/bphen or EML/bphen) that traps electrons, thus hampering the electron transport across the n-OSC as well as an efficient injection of electrons into the EML. The introduction of an additional layer in a structure, that is already optimized in terms of energy level alignment, is therefore critical for the device performance.

Overall, we can conclude that the interplay between energy level alignment, charge transport characteristics of the n-OSC, and the nature of the EML/OSC interface in trilayer OLETs is crucial to achieve optimal performances in terms of ambipolarity and optical power generation. On the one side, OLETs based on P13 as n-OSC show well-balanced charge densities at the expense of poor emission characteristics. Electrons are mostly populating the P13 layer rather than being injected into the EML. The energy level misalignment at the EML/P13 interface is not improved by the implementation of a bphen interlayer, that has a negligible influence on the optical properties of the devices. On the other side, OLETs based on N-F2-6 as n-OSC are characterized by a good energy level alignment of the layers that, in agreement with the high EQE and EL_{max} values, prompts efficient emitting characteristics of the devices. Nevertheless, N-F2-6-based OLETs lack ambipolar

© 2022 The Authors. Advanced Materials Interfaces published by Wiley-VCH GmbH

ADVANCED MATERIALS INTERFACES
www.advmatinterfaces.de

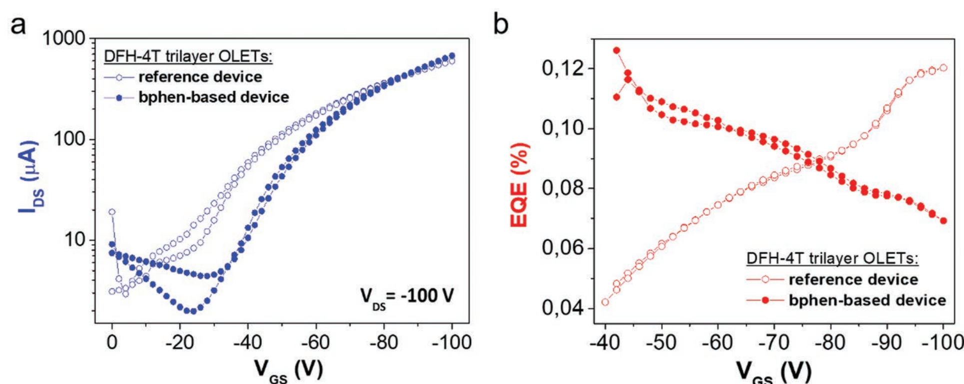

Figure 5. a) P-type transfer curves in saturation regime of DFH-4T-based trilayer OLETs with (filled dots) and without (empty dots) bphen interlayer; b) EQE curves of DFH-4T-based trilayer OLETs with (filled dots) and without (empty dots) bphen interlayer.

characteristics, and further enhancement of either the n-type semiconducting behavior or the electron injection into the EML cannot be obtained by the introduction of an EIL at the EML/N-F2-6 interface.

Thus, DFH-4T was investigated as n-OSC since it is characterized by charge transport properties similar to those of P13 but having a deep HOMO (−6.2 eV) that could prevent the injection of holes from the EML to the n-OSC (Figure 1b). DFH-4T shows indeed a good balance of the optoelectronic properties of the n-OSCs studied herein.

The use of DFH-4T in trilayer OLETs results in devices with a rather unbalanced electrical behavior that is mostly dominated by hole transport, as it can be seen from the unipolar behavior of p-type saturation transfer characteristics (**Figure 5**a). Output curves (**Figure 6**a; Figure S8b,c, Supporting Information) confirm the p-type operation of the device, thus showing a saturation regime of I_{ds} only under negative polarization of the gate dielectric (Figure 6a; Figure S8b, Supporting Information) as well as the absence of any pinch-off points under positive gate bias (Figure S8c, Supporting Information). The benefit of using a n-OSC with a HOMO level lower than that of P13 leads to an improvement of light emission intensity under unipolar operation (V_{gs} = V_{ds} = −100 V) (Table 1). Accordingly, the EQE_{max} is one order of magnitude higher than that of the P13-trilayer OLET (Figures 3b,5b) and increases from 0.012% to 0.12% at V_{gs} = −100 V. With respect to P13-based OLETs, the use of DFH-4T is therefore functional to hamper undesirable hole injection into the DFH-4T layer, which would otherwise hinder exciton formation processes in the EML. Nevertheless, the poor n-type characteristics of DFH-4T-based OLETs limit light emission to occur under unipolar operation, thus avoiding any possibilities to tune the emission region toward the transistor channel.

The deposition of a bphen layer on top of the EML dramatically changes the electrical characteristics of DFH-4T-based OLETs. In particular, p-type saturation transfer characteristics are endowed with both p- and n-type contributions as indicated by a clear V-shape that is absent in the reference device (Figure 5a). The p-type contribution is more pronounced. Despite that, n-type characteristics are clearly visible from the

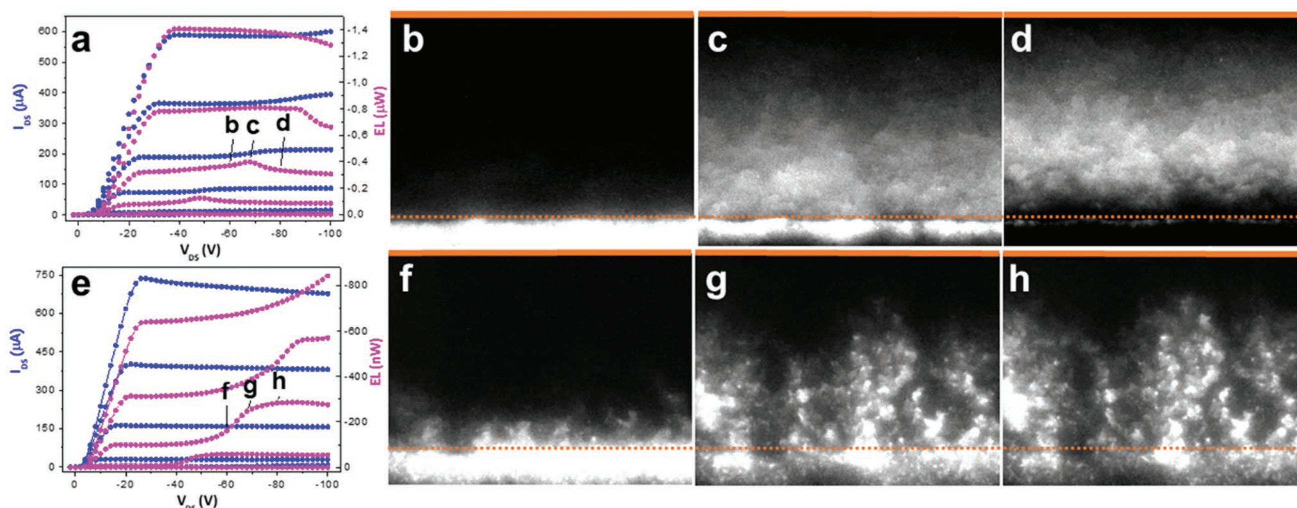

Figure 6. a,e) P-type output curves and b–d,f–h)optical images of reference (a–d) and bphen-based (e–h) DFH-4T-trilayer OLETs. From left to right, optical images refer to V_{gs} = −60 V and V_{ds} = −60, −68, and −80 V as indicated in the corresponding panel (a) and (e). Dotted and solid orange lines indicate the inner edge of the drain and the source electrodes, respectively. Images are recorded through the glass substrate with a 60× magnification. The lateral dimension of the optical images is 120 μm × 80 μm.

© 2022 The Authors. Advanced Materials Interfaces published by Wiley-VCH GmbH

21967350, 2022, 5, Downloaded from https://onlinelibrary.wiley.com/doi/10.1002/admi.202101926 by CNR Bologna, Wiley Online Library on [19/12/2024]. See the Terms and Conditions (https://onlinelibrary.wiley.com/terms-and-conditions) on Wiley Online Library for rules of use; OA articles are governed by the applicable Creative Commons License

21967350, 2022, 5, Downloaded from https://onlinelibrary.wiley.com/doi/10.1002/admi.202101926 by CNR Bologna, Wiley Online Library on [19/12/2024]. See the Terms and Conditions (https://onlinelibrary.wiley.com/terms-and-conditions) on Wiley Online Library for rules of use; OA articles are governed by the applicable Creative Commons License

locus curves in the positive bias region (Figure S8a, Supporting Information). Moreover, although the n-type contribution to the I_{ds} current is not clearly visible from p-type output curves (Figure 6e; Figure S8d, Supporting Information), the formation of the n-type channel can be easily distinguished from n-type output curves at $V_{gs} \geq 80$ V (Figure S8e, Supporting Information, inset), as indicated by the presence of a pinch-off point and the relative saturation regime. Different from the P13-based OLETs, the implementation of a bphen interlayer at the EML/DFH-4T interface improves the n-type characteristics while preserving the p-type behavior of the OLET structure (Table 1). Modifications of the p-type characteristics concern the $V_{th(h)}$ that increases from −11.7 to −30.0 V. This variation could be correlated with enhanced hole injection barrier from the source electrode to the C8-BTBT layer as a result of the additional 0.2 eV of energy offset at the n-OSC/EML interface. In addition to the improved ambipolar characteristics, bphen-based OLETs show an inversion of the EQE trend as a function of V_{gs}, with respect to that of the reference trilayer device (Figure 5b). Under p-type unipolar operation, the reference trilayer OLET shows an increase of the EQE by increasing V_{gs} and the maximum value of 0.12% is obtained at $V_{gs} = V_{ds} = -100$ V. However, when a bphen interlayer is used, the same EQE value is reached at $V_{gs} = -40$ V and then decreases at $V_{gs} = -100$ V (Figure 5b).

Unlike P13- and N-F2-6-based trilayer OLETs, the behavior of devices comprising DFH-4T is unexpected considering the electron mobility of DFH-4T and its energy level alignment within the device structure. Unusual variations of the optical power of emission are also visible during p-type output analyses (Figure 6a,e). In particular, the reference device shows a transient peak of the optical power of emission with increased V_{ds} at $V_{gs} = -60$ V (Figure 6a). Diversely, bphen-based OLETs exhibit a gradual enhancement of the optical power as a function of V_{ds} at $V_{gs} = -60$ V, which reaches a plateau by further increasing V_{ds}. Similar behaviors can be found in the EQE spectra calculated from the p-type output curves of the reference and the bphen-based OLETs (Figure S9, Supporting Information). To deepen into the device operation, the spatial region of emission is visualized as a function of the source-drain bias. In this regard, the optical images of the OLETs are therefore recorded at three different V_{ds} values of −60, −68, and −80 V while keeping a constant V_{gs} of −60 V (Figure 6). In this context, it is worth mentioning that the spectral emission of all OLETs is similar regardless of the type of n-type OSC and the presence of a bphen interlayer (Figure S7, Supporting Information).

At a bias of $V_{gs} = V_{ds} = -60$ V (Figure 6a, point b, and Figure 6e, point f), these OLETs operate in an almost unipolar condition as evidenced by the negligible current that is recorded under the n-type locus characterization (Figure S8a, Supporting Information). Accordingly, both the reference and the bphen-based devices exhibit a pattern of emission that involves the spatial region corresponding to the drain electrode (Figure 6b,f). By increasing V_{ds} from −60 to −68 V (Figure 6a, point c), the light emission of the reference trilayer OLET is expected to remain in the spatial region of the EML underneath the drain electrode as a result of the significant unipolarity of the device. However, the corresponding optical image shows light originating from the transistor channel in conjunction with a residual illumination from the region corresponding to the drain electrode (Figure 6c). The evidence of light emission occurring within the transistor channel is in contrast with assumptions that are based on the transfer and output electrical characteristics of the device. Therefore, it can be speculated that the ambipolarity of the reference DFH-4T-based OLETs hides behind a more pronounced p-type behavior. All electrical curves are characterized by an n-type contribution that is overwhelmed by the p-type behavior. As a result, the emission pattern of OLETs provides a direct fingerprint and it is a more sensitive indicator of the fundamental device electrical characteristics than the standard electrical measurements. The visualization of the bias-dependent optical emission can therefore be implemented as a straightforward method to better identify the intrinsic OLET electrical features.

At $V_{ds} = -68$ V, $V_{gs} = -60$ (Figure 6e, point g), bphen-based OLETs are assumed to operate under a slightly more ambipolar regime than the reference device. Radiative recombination events within the EML must be located between the source and drain electrodes to generate emission within the transistor channel. Diversely, the bphen-based OLETs show a pattern of emission involving both the transistor channel and the drain electrode. Unlike the reference devices, a homogeneous illumination of the full area of the drain electrode can also be noted in bphen-based OLETs. This observation likely suggests that the operation of the bphen interlayer as EIL enables radiative recombination events to occur in the region corresponding to the drain electrode, thus adding up to the light emitted in the OLET channel under this specific bias condition. By further increasing V_{ds} to −80 V, at $V_{gs} = -60$ V, a more pronounced ambipolar regime is generally favored. Charge recombination processes are expected to move gradually from the drain electrode region toward the transistor channel for both devices. The optical power of emission for the reference OLETs is slightly reduced when V_{ds} changes from −60 to −80 V (Figure 6a, point d). Accordingly, a wide emission area in the device channel is visible in the optical images (Figure 6d).

The presence of the bphen interlayer induces light emission both from the transistor channel and the region corresponding to the drain electrode (Figure 6h), as already occurred at $V_{ds} = -68$ V and $V_{gs} = -60$ V (Figure 6g). The main difference with respect to the reference device concerns the emission of light under the drain electrode, that is not expected to occur as the presence of light within the transistor channel is an indication of device ambipolarity. It is indeed known that the emission under the drain electrode is dominant under unipolar regime. The implementation of a bphen interlayer in DFH-4T OLETs therefore promotes the vertical injection of electrons from the drain electrode to the EML that can be ascribed to its operation as an EIL.

The analysis of the pattern of emission under different operational conditions allows evaluating the different trends of the EQE as a function of V_{gs} between reference and bphen-based OLETs (Figure 5b). Basically, in both devices, the unipolar regime of operation is induced at $|V_{ds}| = |V_{gs}|$, while the ambipolar regime occurs when $|V_{ds}| > |V_{gs}|$. As a result, if analyzing the EQE at $V_{ds} = -100$ V and $V_{gs} = -40$ V (Figure 5b), the ambipolar regime of operation occurs in both devices and hence their emission patterns is expected to resemble that shown in Figure 6d,h. An improved electron injection into the

 © 2022 The Authors. Advanced Materials Interfaces published by Wiley-VCH GmbH

EML in bphen-based OLETs is therefore at the origin of the EQE enhancement with respect to the reference device since an additional region of emission, that is, region under the drain electrode, is activated.

An increase of V_{gs} up to –100 V, at V_{ds} of –100 V (Figure 5a) induces both OLETs to gradually switch from ambipolar to unipolar operation. The pattern of emission of both devices at $V_{ds} = V_{gs} = -100$ V is expected to be similar to that shown in Figure 6b,f because of the similarity of the operational conditions (i.e., $V_{ds} = V_{gs} = -60$ V, unipolar regime). Therefore, light emission is in the region of the EML corresponding to the drain electrode for both reference and bphen-based OLETs. Given that the pattern of emission is similar and EQE values are different, it is likely that the use an EIL enables a diode-like behavior of the device in which quenching mechanisms, such as exciton-charge annihilation, occur.

By analyzing optical images, it is also evident the presence of a coarser pattern of emission in bphen-based OLETs in contrast to a more regular one in reference devices (Figure 6c,d,g,h). This morphological difference can be analyzed in depth by AFM analyses (**Figure 7**).

It is worth noting that the morphology of the DFH-4T film when it is directly deposited onto the EML is not as homogeneous as it typically occurs when the film is formed on a flat surface.[10] Rather than 2D islands, the growth of the DFH-4T film onto the EML shows indeed the tendency of DFH-4T to aggregate in 3D domains (height ≈ 50 nm). The formation of a different morphology is most probably at the origin of the poor ambipolar characteristics of DFH-4T-based OLETs.

More interestingly, a significant change of the surface organization of DFH-4T occurs when it is deposited onto the bphen layer. While the reference device shows 3D motifs of DFH-4T (Figure 7a), filamentary structures a few micrometers long of DFH-4T develop onto the layer of bphen (Figure 7b). The presence of a bphen interlayer likely induces DFH-4T to form long percolative pathways. From an electrical point of view, this effect explains the increase of the lateral electron transport through the DFH-4T layer, which leads to a more balanced ambipolar behavior of bphen-based OLETs with respect to reference devices. The correlation between an increase of the ambipolarity and a high EQE under ambipolar regime in bphen-based OLETs suggests that a greater number of electrons flows in the DFH-4T layer and it is more effectively injected into the EML in comparison with the reference device. Overall, the introduction of a bphen interlayer in DFH-4T OLETs has the dual benefit of i) extending the spatial area of emission by keeping the region under the drain electrode active even under ambipolar operation, and ii) improving the number of recombination events as well as the formation of lateral percolative pathways in the n-OSC film. Therefore, the implementation of a bphen interlayer in the DFH-4T trilayer OLETs allows reaching wider emissive areas and high EQE values at a lower applied bias. For instance, the use of a V_{gs} as low as –40 V is sufficient to enhance the EQE of bphen-based OLETs by ≈2× than those obtained in reference devices (Figure S9, Supporting Information).

Although a further improved balance of electron and hole mobilities is needed for trilayer OLETs with optimum performance, it is clear that the combination of long-range lateral transport, morphology and vertical injection determines the behavior of this kind of bidimensional multilayer structures.

3. Conclusion

The multitude of factors contributing to the operation of ambipolar trilayer OLETs hinders an optimal design of the device structure. Our comparative work elucidates the role and the interplay between intrinsic optoelectronic characteristics, energy level alignment and morphological factors on the performance of this class of devices. The use of P13 and N-F2-6 as n-OSC layer on top of the EML confirmed the importance of the energy level alignment and the need of well-balanced charge transport characteristics in trilayer OLETs. Nevertheless, interfacial properties at the EML/n-OSC are important for optimizing charge transport and light generation in DFH-4T-based OLETs. Indeed, suboptimal 3D morphology of the DFH-4T film on top of the EML reduced n-OSC electron transport and induced a unipolar p-type operation of the corresponding devices. The introduction of a bphen interlayer at the EML/DFH-4T interface improved the solid-state organization of the DFH-4T layer thus favoring ambipolarity. Under this operational regime, the increase of the number of electrons in conjunction with their efficient vertical injection into the EML due to the bphen interlayer allowed a ≈2× improvement of the

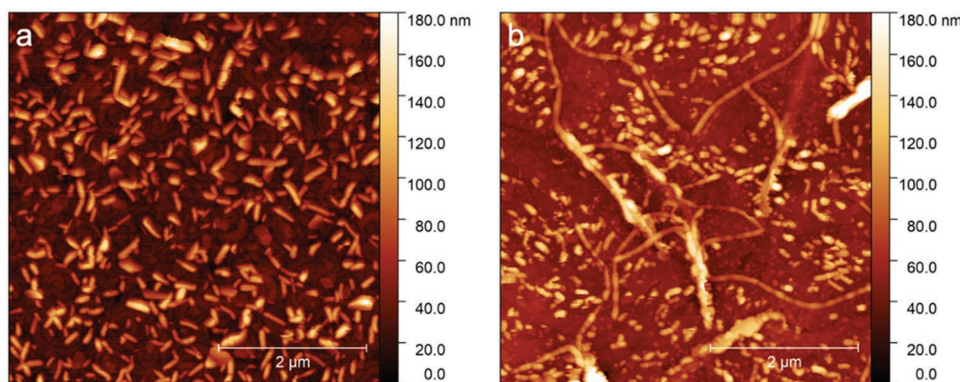

Figure 7. AFM images of DFH-4T recorded within the corresponding OLET channel of the a) reference and b) bphen-based devices. Lateral dimensions: 5µm. Calculated RMS is 26 nm for both devices.

© 2022 The Authors. Advanced Materials Interfaces published by Wiley-VCH GmbH

21967350, 2022, 5, Downloaded from https://onlinelibrary.wiley.com/doi/10.1002/admi.202101926 by CNR Bologna, Wiley Online Library on [19/12/2024]. See the Terms and Conditions (https://onlinelibrary.wiley.com/terms-and-conditions) on Wiley Online Library for rules of use; OA articles are governed by the applicable Creative Commons License

ADVANCED MATERIALS INTERFACES
www.advmatinterfaces.de

device EQE at a reduced operational bias. Thus, on one side, the use of a bphen interlayer expanded the OLET emissive area and the geometrical fill factor, as it is desired for pixel design in display applications.[43] On the other side, the implementation of a vertical electron injecting layer, that is typical of OLED structures, in a bidimensional OLET device further extends the library of materials that can be implemented in OLETs.

The pivotal importance of interfaces in multilayered optoelectronic devices, in addition to the bidimensional nature of the OLET trilayer heterostructure, highlights the need for a better control of the operational mechanisms occurring at the two EML/OSCs interfaces. While an extended library of n-OSC is needed to improve the OLET electrical ambipolarity, an accurate selection of vertical injecting interlayers to be included at the EML/n-OSC (p-OSC) interface is strongly recommended. In this context, the bias-dependent pattern of emission provides a direct fingerprint and a more sensitive method to evaluate the OLET ambipolarity with respect to the standard analysis of the device electrical characteristics.

4. Experimental Section

Device Fabrication: All trilayer OLET heterostructures were fabricated in bottom-gate/top-contact configuration (Figure 1a). The substrates consisted of 25 × 25 mm glass coated with a 120 nm thick patterned ITO serving as gate electrode. A film of 450 nm of PMMA was spin-coated on the substrate as dielectric layer in according to the literature procedure in ref. [44]. The basic structure was composed of stacked bilayer of i) 45 nm of p-type semiconductor C8-BTBT sublimed at 0.1 Å s^{-1} and ii) a 30 nm thick host-guest EML of Alq_3 (host) and Pt(tpbp) (guest) (doping percentage: 6%) sublimed at 3 and 0.2 Å s^{-1}, respectively. The n-type semiconductors sublimed on the bilayer structure were 15 nm of P13, 45 nm of N-F2-6, and 25 nm of DFH-4T, all sublimed at 0.1 Å s^{-1}. A 5 nm thick Bphen interlayer was sublimated at the n-type semiconductors/EML interface at 0.3 Å s^{-1}. The organic trilayer stack was then covered by a 70 nm thick source and drain silver electrodes deposited by thermal evaporation using shadow masks. Both the electrodes and the organic layers were grown at a base pressure of 2.7×10^{-7} mbar, in a K. J. Lesker chamber directly connected to the nitrogen glove box to prevent sample exposure to air during each step of the device realization. For optical imaging measurements, devices were encapsulated by using a transparent glass cap and a UV-curable glue (UV-Resin XNR5516Z-B1, Nagase). The resulting devices presented the following characteristics: 12 mm channel width (W), 70 µm channel length (L), and 500 µm wide source and drain electrodes. P13 an DFH-4T were purchased from Sigma Aldrich and Lumtec, respectively, and used without further purification. N-F2-6 was synthesized in accordance with a previously reported procedure in ref. [45].

Optoelectronic Characterization: The electrical and optical measurements were performed in an inert atmosphere inside a nitrogen-filled glovebox using a standard SUSS probe station coupled to a B1500A Agilent semiconductor device analyzer. The light output was measured at the bottom side of the substrates (i.e., through the gate electrode) with a silicon photodiode (a sensitivity of 0.38 A W^{-1} at 600 nm) directly in contact with the devices to enable the collection of all emitted photons.

The EQE was calculated directly as the ratio between the total emitted photons and the charge flow that formed the drain current. The field-effect mobilities in the saturation regime ($\mu_{(e)} - \mu_{(h)}$) were calculated using the equation $I_{ds} = (W/2L)C_i\mu(V_{gs} - V_{th})^2$, where C_i is the capacitance per unit area of the insulating layer and V_{th} is the threshold voltage extracted from the square root of the drain current ($I_{ds}^{1/2}$) versus gate voltage (V_{gs}) characteristics.

Electroluminescence spectra of devices biased using a Keithley 2602B were acquired by a Hamamatsu multichannel optical analyzer (PMA11).

Photoluminescence quantum yield measurements of EMLs on quartz substrates were carried out inside a 6 in. integrating sphere optically coupled to a Hamamatsu PMA optical multichannel analyzer by exciting photoluminescence at 442 nm according to absorption maxima of the samples.

Optical Imaging: Optical imaging of the devices channels and recombination regions were recorded with a Nikon Eclipse 2000-E microscope on encapsulated OLETs, using a sample holder equipped with electrical connections that placed the optoelectronic devices in the focal plane of the microscope. Optical detection was achieved using 60× magnification objective and a Hamamatsu high-resolution digital camera coupled to a B1500A Agilent semiconductor device analyzer to drive the devices.

AFM: Topographic AFM measurements of trilayer devices were performed in ScanAsyst mode using Bruker SNL-10 probes on Bruker Multimode 8 microscope with a Nanoscope V controller and J scanner. All measurements were performed in the air onto sacrificial devices.

Supporting Information

Supporting Information is available from the Wiley Online Library or from the author.

Acknowledgements

This work had received funding from the European Union's Horizon 2020 Research and Innovation Programme under grant agreement No 101016706 (h-ALO). The authors thank Federico Prescimone and Vincenzo Ragona for the valuable technical support.

Conflict of Interest

The authors declare no conflict of interest.

Data Availability Statement

The data that support the findings of this study are available from the corresponding author upon reasonable request.

Keywords

ambipolar trilayer heterostructure, electron injection layer, external quantum efficiency, n-type organic semiconductors, organic light-emitting transistors, wide area emission

Received: October 6, 2021
Revised: November 12, 2021
Published online: January 15, 2022

[1] H. Sirringhaus, *Adv. Mater.* **2014**, *26*, 1319.
[2] G. Gelinck, P. Heremans, K. Nomoto, T. D. Anthopoulos, *Adv. Mater.* **2010**, *22*, 3778.
[3] J. Zaumseil, *Adv. Funct. Mater.* **2020**, *30*, 1905269.
[4] M. Prosa, M. Bolognesi, L. Fornasari, G. Grasso, L. Lopez-Sanchez, F. Marabelli, S. Toffanin, *Nanomaterials* **2020**, *10*, 480.
[5] Y. Huang, E.-L. Hsiang, M.-Y. Deng, S.-T. Wu, *Light: Sci. Appl.* **2020**, *9*, 105.

 © 2022 The Authors. Advanced Materials Interfaces published by Wiley-VCH GmbH

21967350, 2022, 5, Downloaded from https://onlinelibrary.wiley.com/doi/10.1002/admi.202101926 by CNR Bologna, Wiley Online Library on [19/12/2024]. See the Terms and Conditions (https://onlinelibrary.wiley.com/terms-and-conditions) on Wiley Online Library for rules of use; OA articles are governed by the applicable Creative Commons License

21967350, 2022, 5, Downloaded from https://onlinelibrary.wiley.com/doi/10.1002/admi.202101926 by CNR Bologna, Wiley Online Library on [19/12/2024]. See the Terms and Conditions (https://onlinelibrary.wiley.com/terms-and-conditions) on Wiley Online Library for rules of use; OA articles are governed by the applicable Creative Commons License

[6] M. Muccini, S. Toffanin, *Organic Light-Emitting Transistors: Towards the Next Generation Display Technology*, Wiley, New York **2016**.
[7] H. F. Wittmann, J. Grüner, R. H. Friend, G. W. C. Spencer, S. C. Moratti, A. B. Holmes, *Adv. Mater.* **1995**, *7*, 541.
[8] J. Feng, Y.-F. Liu, Y.-G. Bi, H.-B. Sun, *Laser Photonics Rev.* **2017**, *11*, 1600145.
[9] M. Muccini, *Nat. Mater.* **2006**, *5*, 605.
[10] R. Capelli, S. Toffanin, G. Generali, H. Usta, A. Facchetti, M. Muccini, *Nat. Mater.* **2010**, *9*, 496.
[11] S. Toffanin, R. Capelli, W. Koopman, G. Generali, S. Cavallini, A. Stefani, D. Saguatti, G. Ruani, M. Muccini, *Laser Photonics Rev.* **2013**, *7*, 1011.
[12] M. Natali, S. D. Quiroga, L. Passoni, L. Criante, E. Benvenuti, G. Bolognini, L. Favaretto, M. Melucci, M. Muccini, F. Scotognella, F. Di Fonzo, S. Toffanin, *Adv. Funct. Mater.* **2017**, *27*, 1605164.
[13] M. Prosa, E. Benvenuti, D. Kallweit, P. Pellacani, M. Toerker, M. Bolognesi, L. Lopez-Sanchez, V. Ragona, F. Marabelli, S. Toffanin, *Adv. Funct. Mater.* **2021**, *31*, 2104927.
[14] R. Capelli, F. Dinelli, S. Toffanin, F. Todescato, M. Murgia, M. Muccini, A. Facchetti, T. J. Marks, *J. Phys. Chem. C* **2008**, *112*, 12993.
[15] M. Melucci, M. Zambianchi, L. Favaretto, M. Gazzano, A. Zanelli, M. Monari, R. Capelli, S. Troisi, S. Toffanin, M. Muccini, *Chem. Commun.* **2011**, *47*, 11840.
[16] M. Melucci, L. Favaretto, M. Zambianchi, M. Durso, M. Gazzano, A. Zanelli, M. Monari, M. G. Lobello, F. De Angelis, V. Biondo, G. Generali, S. Troisi, W. Koopman, S. Toffanin, R. Capelli, M. Muccini, *Chem. Mater.* **2013**, *25*, 668.
[17] M. Prosa, S. Moschetto, E. Benvenuti, M. Zambianchi, M. Muccini, M. Melucci, S. Toffanin, *J. Mater. Chem. C* **2020**, *8*, 15048.
[18] M. Muccini, W. Koopman, S. Toffanin, *Laser Photonics Rev.* **2012**, *6*, 258.
[19] D. Yuan, M. A. Awais, V. Sharapov, X. Liu, A. Neshchadin, W. Chen, M. Bera, L. Yu, *Chem. Sci.* **2020**, *11*, 11315.
[20] M. Ullah, K. Tandy, S. D. Yambem, M. Aljada, P. L. Burn, P. Meredith, E. B. Namdas, *Adv. Mater.* **2013**, *25*, 6213.
[21] Y. Yuan, G. Giri, A. L. Ayzner, A. P. Zoombelt, S. C. B. Mannsfeld, J. Chen, D. Nordlund, M. F. Toney, J. Huang, Z. Bao, *Nat. Commun.* **2014**, *5*, 3005.
[22] C. Luo, A. K. K. Kyaw, L. A. Perez, S. Patel, M. Wang, B. Grimm, G. C. Bazan, E. J. Kramer, A. J. Heeger, *Nano Lett.* **2014**, *14*, 2764.
[23] C. R. Newman, C. D. Frisbie, D. A. da Silva Filho, J.-L. Brédas, P. C. Ewbank, K. R. Mann, *Chem. Mater.* **2004**, *16*, 4436.
[24] X. Gao, Y. Hu, *J. Mater. Chem. C* **2014**, *2*, 3099.
[25] X. Zhao, X. Zhan, *Chem. Soc. Rev.* **2011**, *40*, 3728.
[26] Y. Zhao, Y. Guo, Y. Liu, *Adv. Mater.* **2013**, *25*, 5372.
[27] J. E. Anthony, A. Facchetti, M. Heeney, S. R. Marder, X. Zhan, *Adv. Mater.* **2010**, *22*, 3876.
[28] J. Zaumseil, H. Sirringhaus, *Chem. Rev.* **2007**, *107*, 1296.
[29] J. Sobus, F. Bencheikh, M. Mamada, R. Wawrzinek, J. Ribierre, C. Adachi, S. Lo, E. B. Namdas, *Adv. Funct. Mater.* **2018**, *28*, 1800340.
[30] L. Song, Y. Hu, D. Li, H. Chen, X. Liu, *J. Phys. Chem. C* **2015**, *119*, 20237.
[31] C. Borek, K. Hanson, P. I. Djurovich, M. E. Thompson, K. Aznavour, R. Bau, Y. Sun, S. R. Forrest, J. Brooks, L. Michalski, J. Brown, *Angew. Chem.* **2007**, *46*, 1109.
[32] M. Natali, M. Prosa, A. Longo, M. Brucale, F. Mercuri, M. Buonomo, N. Lago, E. Benvenuti, F. Prescimone, C. Bettini, A. Cester, M. Melucci, M. Muccini, S. Toffanin, *ACS Appl. Mater. Interfaces* **2020**, *12*, 30616.
[33] H. Usta, C. Risko, Z. Wang, H. Huang, M. K. Deliomeroglu, A. Zhukhovitskiy, A. Facchetti, T. J. Marks, *J. Am. Chem. Soc.* **2009**, *131*, 5586.
[34] S. Bonetti, M. Prosa, A. Pistone, L. Favaretto, A. Sagnella, I. Grisin, M. Zambianchi, S. Karges, A. Lorenzoni, T. Posati, R. Zamboni, N. Camaioni, F. Mercuri, M. Muccini, M. Melucci, V. Benfenati, *J. Mater. Chem. B* **2016**, *4*, 2921.
[35] G. Generali, C. Soldano, A. Facchetti, M. Muccini, *SID Symp. Dig. Tech. Pap.* **2016**, *47*, 1779.
[36] G. Generali, F. Dinelli, R. Capelli, S. Toffanin, M. Muccini, *J. Phys. D: Appl. Phys.* **2011**, *44*, 224018.
[37] V. Ahmad, J. Sobus, F. Bencheikh, M. Mamada, C. Adachi, S.-C. Lo, E. B. Namdas, *Adv. Opt. Mater.* **2020**, *8*, 2000554.
[38] J. G. Jang, H. J. Ji, H. S. Kim, J. C. Jeong, *Curr. Appl. Phys.* **2011**, *11*, S251.
[39] M. Prosa, E. Benvenuti, M. Pasini, U. Giovanella, M. Bolognesi, L. Meazza, F. Galeotti, M. Muccini, S. Toffanin, *ACS Appl. Mater. Interfaces* **2018**, *10*, 25580.
[40] G. Paasch, T.h. Lindner, C. Rost-Bietsch, S. Karg, W. Riess, S. Scheinert, *J. Appl. Phys.* **2005**, *98*, 084505.
[41] H. Chen, W. Huang, T. J. Marks, A. Facchetti, H. Meng, *Small* **2021**, *17*, 2007661.
[42] Y. Ren, X. Yang, L. Zhou, J. Mao, S. Han, Y. Zhou, *Adv. Funct. Mater.* **2019**, *29*, 1902105.
[43] P. Ganesan, H. N. Tsao, P. Gao, *Adv. Funct. Mater.* **2021**, *31*, 2105506.
[44] M. Zambianchi, E. Benvenuti, C. Bettini, C. Zanardi, R. Seeber, D. Gentili, M. Cavallini, M. Muccini, V. Biondo, C. Soldano, G. Generali, S. Toffanin, M. Melucci, *J. Mater. Chem. C* **2016**, *4*, 9411.
[45] A. Facchetti, H. Usta, M. Denti, V. Biondo, C. Soldano, M. Muccini, WO2016014973, **2016**.

© 2022 The Authors. Advanced Materials Interfaces published by Wiley-VCH GmbH